ELSEVIER

Journal of Molecular Catalysis A: Chemical 152 (2000) 157–165

JOURNAL OF MOLECULAR CATALYSIS A: CHEMICAL

www.elsevier.com/locate/molcata

Catalytic methanol decomposition to carbon monoxide and hydrogen over nickel supported on silica

Yasuyuki Matsumura *, Koji Tanaka, Naoki Tode, Tetsuo Yazawa, Masatake Haruta

Osaka National Research Institute, AIST, 1-8-31 Midorigaoka, Ikeda, Osaka 563-8577, Japan

Received 28 January 1999; accepted 2 July 1999

Abstract

The decomposition of methanol to carbon monoxide and hydrogen can be catalyzed at 250°C over nickel supported on silica. The activity of the catalyst prepared by a sol–gel method increases with an increase in the content of nickel up to 40 wt.% while that for the sample prepared by an impregnation technique almost reaches a plateau at the nickel content of 10 wt.%. The activity does not relate simply to the nickel surface area of the sample, but it depends on the amounts of carbon monoxide and hydrogen strongly adsorbed on the catalyst. Small nickel particles are disadvantageous in the reaction.

Keywords: Methanol decomposition; Sol–gel method; Nickel; Adsorption

1. Introduction

Methanol is expected as a new liquid energy carrier because it can be synthesized from biomass, coal, and natural gas all of which will be more abundant resources than crude oil [1,2]. The decomposition of methanol to carbon monoxide and hydrogen is attracting a growing interest for use of methanol-fuelled vehicles in which the heat of exhaust gas is recovered by the endothermic reaction and the decomposition gas is fed to the engine [3]. The reaction is also applicable to the recovery of waste heat from industries, but significant improvement of the catalysts must be achieved.

Catalysts containing nickel have been reported to be active for methanol decomposition [4–23]. Since the activity of supported nickel catalysts should depend on the surface area of the metal, the content and particle size of nickel on the surface are important factors in determining the activity while other physical and chemical properties such as electronic state of nickel cannot be ignored [24–27].

In this work nickel supported on silica with different nickel contents were prepared by sol–gel and impregnation methods. We carried out characterization of the catalysts as well as the catalytic test for the methanol decomposition and, interestingly, the investigation shows that

* Corresponding author. Tel.: +81-727-51-9652; fax: +81-727-51-9629; E-mail: yasumatsumura@onri.go.jp

1381-1169/00/$ - see front matter
PII: S1381-1169(99)00282-4

small nickel particles are less active than large ones.

2. Experimental

Six samples of nickel supported on silica were prepared by hydrolysis and polymerization of the mixture of tetraethyl orthosilicate (GR grade, Kanto Chemical), nickel nitrate (GR, Kanto), nitric acid (GR, Kanto), ethanol, and water. After drying in air at 120°C the solid was heated in air for 5 h at 400°C for removal of NO_3^- anions and residual organic compounds. The samples contained 5–50 wt.% of nickel as metal (designated as 5–50 wt.%Ni–S). Some other samples containing 5–20 wt.% of nickel were prepared by impregnation of silica synthesized by the sol–gel method with nickel nitrate. After the impregnation they were heated in air at 400°C for 5 h (5–20 wt.%Ni–I).

The catalytic experiments were performed in a fixed-bed continuous flow reactor operated under an atmospheric pressure. The catalyst was sandwiched with quartz wool plugs in a tube reactor made of stainless steel whose contribution to the reaction was negligible. After reducing the sample (1.0 g) in a flow of hydrogen diluted with argon (H_2, 1.8 $dm^3\ h^{-1}$; Ar, 9.0 $dm^3\ h^{-1}$) for 1 h at 500°C, the catalyst was kept at 250°C under a stream of argon (9.0 $dm^3\ h^{-1}$); then, 3.0 $dm^3\ h^{-1}$ of methanol gas was added to the argon stream. The reactant and products were analyzed with an on-stream Ohkura 802 gas chromatograph equipped with a TC detector. Two columns, one activated carbon (2 m, Ar carrier) and the other Porapak T (2 m, He carrier), were employed.

Powder X-ray diffraction (XRD) patterns were recorded on a Rigaku Rotaflex 20 diffractometer using nickel-filtered CuK_α radiation. Patterns were recorded over the range $2\theta = 3°$–60°. The samples were taken out from the reactor after the reactions of 2 h on-stream. The mean crystallite size of nickel metal or nickel oxide in the sample was determined from widths of the XRD peaks using the equation of Sherrer [28].

Surface analyses by XPS were carried out using a Shimadzu ESCA 750. The samples taken from the reactor after the reaction were mounted on a sample holder in air and set into the spectrometer. Argon-ion sputtering of the sample was carried out (2 kV, 0.5 min) just before the measurement for removal of oxygen adsorbed on the sample. The XPS data were calibrated by assuming that the binding energy of the C 1s peak is 284.6 eV [29].

Infrared (IR) spectrum of a sample dispersed in a KBr wafer was recorded with a JASCO FT/IR 230 spectrometer at room temperature in air.

Transmission electron microscopy (TEM) was carried out with a Hitachi H-9000 operated at an accelerating voltage of 300 kV with a magnification of 10^5.

The BET surface areas of the catalysts after the reaction were determined by nitrogen physisorption with a Quantasorb.JR (Yuasa Ionics).

Adsorption of carbon monoxide and hydrogen was carried out in a vacuum system equipped with Baratron pressure gauges at room temperature. Just before the adsorption, a fresh sample was reduced with hydrogen (ca. 20 kPa) at 500°C for 1 h and evacuated at the same temperature for 0.5 h.

3. Results

3.1. Decomposition of methanol

Methanol decomposed mainly to carbon monoxide and hydrogen over the nickel catalysts at 250°C. Methane and water were also detected as by-products. As shown in Fig. 1, the activity of 5 wt.%Ni–I, which was prepared by the impregnation technique, was higher than that of 5 wt.%Ni–S, a sol–gel sample containing the same quantity of nickel. The activity of the catalyst prepared by the sol–gel method increased with an increase in the nickel content

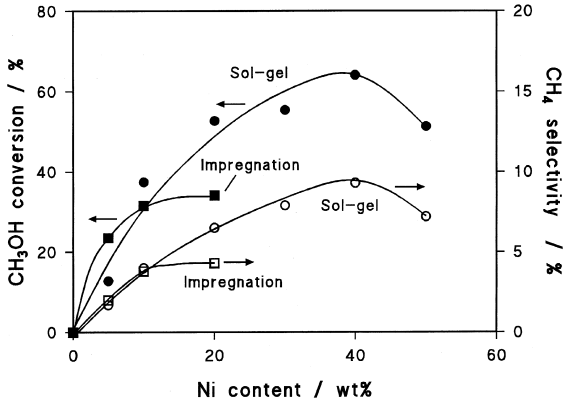

Fig. 1. Methanol decomposition over nickel supported on silica at 250°C.

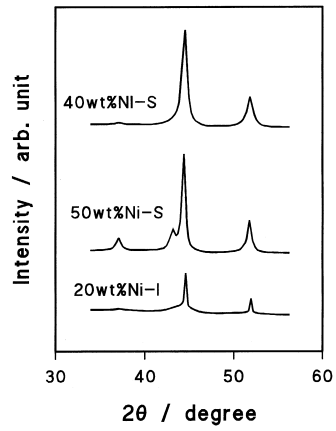

Fig. 2. XRD patterns for the typical samples of nickel supported on silica after reaction.

up to 40 wt.% while the activity of the catalyst prepared by the impregnation method almost reached plateau at the content of 10 wt.%; it can be seen that 20 wt.%Ni–I produced significantly lower conversion than 20 wt.%Ni–S. The selectivity to methane increased with an increase in the conversion of methanol (see Fig. 1), indicating that the formation of methane takes place after the decomposition to carbon monoxide and hydrogen.

3.2. Physical properties of the catalysts

The BET surface area of the catalyst prepared by the sol–gel method increased with increasing content of nickel up to 30 wt.% (471 $m^2\ g^{-1}$), above which it decreased (Table 1). The area for 5 wt.%Ni–I was 553 $m^2\ g^{-1}$ while those for the impregnated catalysts decreased with an increase in the content of nickel.

Peaks attributed to metallic nickel were recorded in the XRD patterns at 44.3° [Ni(111)] and 51.7° [Ni(200)] in 2θ for the catalysts taken out from the reactor after the reaction [30]. The typical patterns are shown in Fig. 2. The crystallite sizes of nickel were determined from the widths of the peak at 44.3° except for 50 wt.%Ni–S (Table 1). In the pattern of 50 wt.%Ni–S, the peaks at 37.3° and 43.3° at-

Table 1
Surface properties of Ni/SiO_2

Catalyst	Surface area (m^2 g)	Crystallite size of Ni (nm)	Binding energy of Ni $2p_{5/2}$		Intensity ratio[a]
			Sharp	Broad	I_{broad}/I_{sharp}
5 wt.%Ni–S	317	2.1	853.1	856.4	1.0
5 wt.%Ni–S[b]			853.0	855.9	1.3
10 wt.%Ni–S	421	5.2	853.0	856.2	0.7
20 wt.%Ni–S	458	7.3	852.9	856.3	1.0
30 wt.%Ni–S	471	10	853.0	856.0	0.9
40 wt.%Ni–S	377	14	852.8	855.7	1.0
50 wt.%Ni–S	352	16	852.8	855.3	2.6
5 wt.%Ni–I	553	4.3	853.0	855.6	1.2
10 wt.%Ni–I	493	5.8	853.0	855.6	0.8
20 wt.%Ni–I	438	4 and 30	853.0	855.9	0.9

[a] Intensity ratio of the broad XPS peak to the sharp one.
[b] 5 wt.%Ni–S after Ar-ion sputtering for 5 min.

tributed to nickel oxide coexist clearly with the peaks for metallic nickel (30), and the crystallite sizes of metallic nickel (16 nm) and nickel oxide (13 nm) were determined from the peaks at 51.7° and 37.3°, respectively. In the patterns of the other samples a small peak was observed at 37°. In the case of 20 wt.%Ni–I, the shape of the peak at 44.3° showed overlap of a sharp peak and a broad one. After deconvolution of these peaks, the crystallite sizes were determined as 4 and 30 nm.

The TEM observation of nickel particles was carried out with the two typical samples, 40 wt.%Ni–S and 20 wt.%Ni–I. In the photographs of the former sample (e.g., Fig. 3) nickel particles with the size around 3–30 nm (dark spots in the photograph) were randomly present. A large particle (ca. 30 nm) was seen in Fig. 4 for 20 wt.%Ni–I; however, small particles with diameter smaller than 5 nm were also observed.

3.3. Surface analyses by XPS

The nickel catalysts taken out just after the reaction were analyzed by XPS. The spectra for Ni $2p_{3/2}$ were separated into two Gaussian peaks and the typical spectra are shown in Fig. 5. The binding energies of the sharp peaks were close to 853 eV regardless of the samples, while the broad peaks were at 855.5–856.4 eV (see Table 1). The intensity ratios of the broad and sharp peaks are also given in Table 1. The shapes of the spectra were not significantly changed after argon-ion sputtering for 5 min (see Fig. 5 for 5 wt.%Ni–S). The binding energies of Si 2p and O 1s were 103.0–103.3 eV and 532.7–532.8 eV for all the samples, respectively.

3.4. IR spectra for Ni/SiO_2

In the IR spectra for the nickel catalysts after reaction, an absorption band at 960 cm^{-1} was

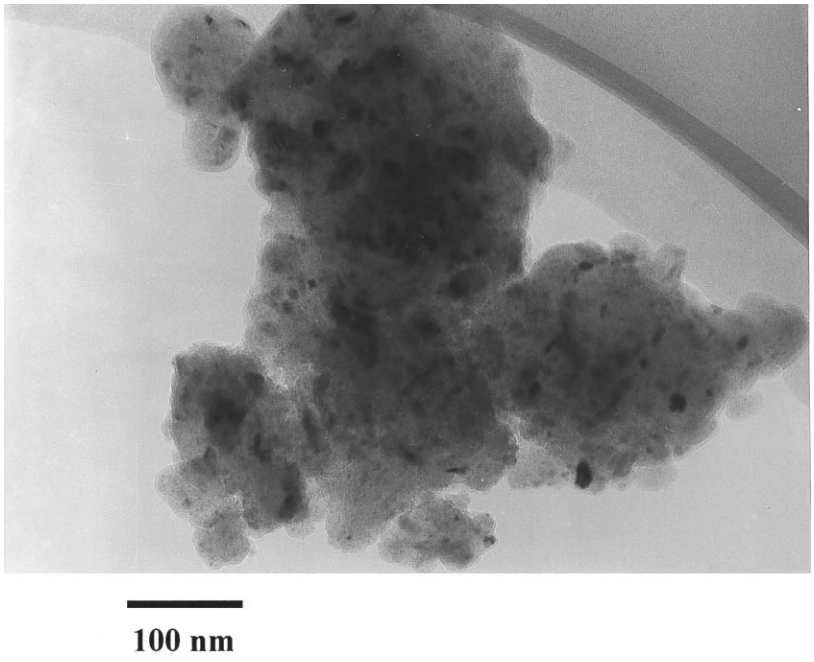

Fig. 3. TEM of 40 wt.%Ni–S after reaction.

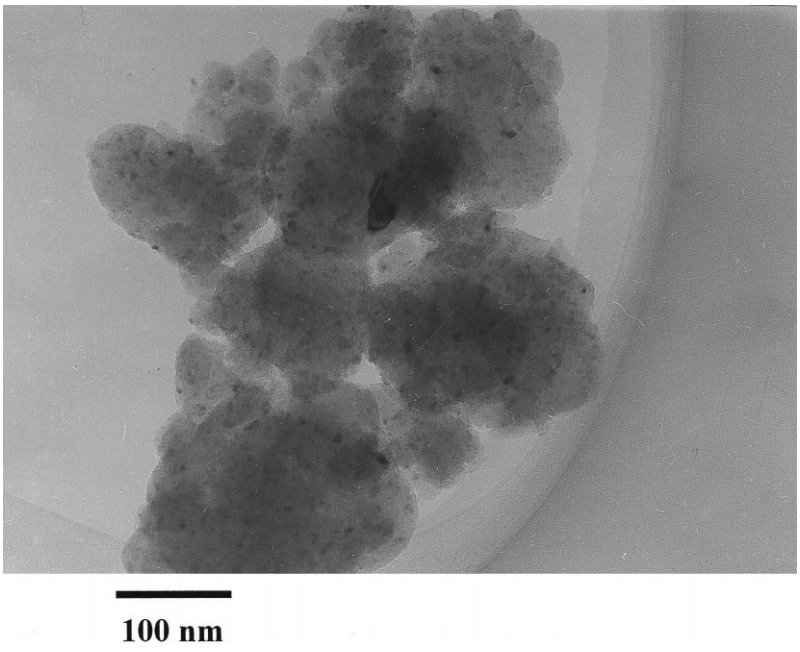

Fig. 4. TEM of 20 wt.%Ni–I after reaction.

observed regardless of the samples. The band can be attributed to Ni–O–Si [26,31]. The bands at 1080 and 802 cm^{-1} are assigned as vibrations of Si–O–Si [32]. The typical spectra are shown in Fig. 6.

3.5. Adsorption of hydrogen and carbon monoxide

Adsorption of hydrogen was carried out at room temperature with the samples reduced at 500°C for 1 h. The typical adsorption isotherms are shown in Fig. 7. The isotherms fit well with an equation of $v = v_{H_2} + aP_{H_2}^{1/2}/(1 + bP_{H_2}^{1/2})$ when the pressure of hydrogen was less than 3 kPa (v, amount of hydrogen adsorbed; v_{H_2}, amount of hydrogen strongly adsorbed; P_{H_2}, pressure of hydrogen; a and b, constants). When the pressure of hydrogen was more than 3 kPa, an equation of $v = c + dP_{H_2}^{1/2}$ showed a good

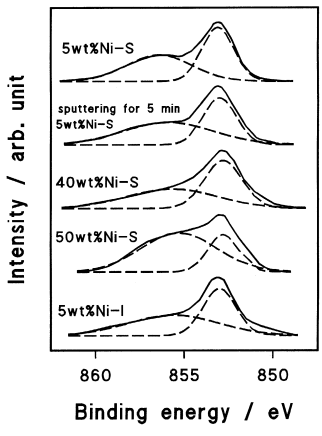

Fig. 5. XPS for the typical samples of nickel supported on silica after reaction.

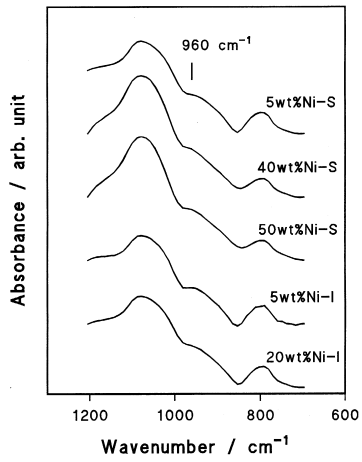

Fig. 6. IR spectra for the typical samples of nickel supported on silica after reaction.

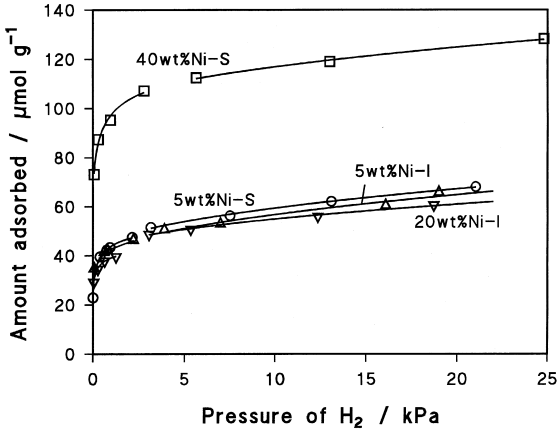

Fig. 7. Typical adsorption isotherms of hydrogen on nickel supported on silica. The curves and lines in the figure are drawn by the curve fitting described in the text.

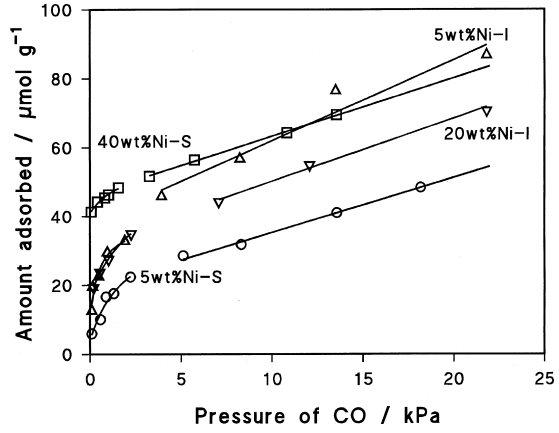

Fig. 8. Typical adsorption isotherms of carbon dioxide on nickel supported on silica. The curves and lines in the figure are drawn by the curve fitting described in the text.

fitting. The amounts of hydrogen strongly adsorbed (v_{H_2}) and those at the pressure of 20 kPa are listed in Table 2. The values of v_{H_2} corresponded well to the amounts of hydrogen irreversibly adsorbed which were determined by the following adsorption after evacuation at room temperature for 0.5 h. The surface area of nickel was determined from the amount of hydrogen adsorbed at 20 kPa (see Table 2) assuming that the surface stoichiometry of one hydrogen atom per nickel atom and the value of 0.0633 nm^2 $atom^{-1}$ as the average surface nickel cross-section [33].

The typical adsorption isotherms for carbon monoxide at room temperature are shown in Fig. 8. The isotherms fit well with an equation of $v = v_{CO} + aP_{CO}/(1 + bP_{CO})$ when the pressure of carbon monoxide was less than 3 kPa (v, amount of carbon monoxide adsorbed; v_{CO}, amount of carbon monoxide strongly adsorbed; P_{CO}, pressure of carbon monoxide; a and b, constants). When the pressure of carbon monoxide was higher than 3 kPa, an equation of $v = c + dP_{CO}$ was applicable. The values of v_{CO} corresponded well to the amounts of carbon monoxide irreversibly adsorbed which were determined by the following adsorption after evac-

Table 2
Adsorption of hydrogen and carbon monoxide on Ni/SiO_2 at room temperature

Sample	Amount adsorbed (μmol g-cat^{-1})				Surface area of nickel (m^2 g-cat^{-1})
	Strong		At 20 kPa		
	H_2 (v_{H_2})	CO (v_{CO})	H_2	CO	
5 wt.%Ni–S	18	4	67	51	5.1
10 wt.%Ni–S	36	14	74	62	5.6
20 wt.%Ni–S	50	24	93	86	7.1
30 wt.%Ni–S	48	24	123	99	9.3
40 wt.%Ni–S	52	41	125	80	9.5
50 wt.%Ni–S	59	35	147	95	11.2
5 wt.%Ni–I	29	10	65	85	4.9
10 wt.%Ni–I	27	18	71	85	5.4
20 wt.%Ni–I	20	17	61	68	4.6

uation at room temperature for 0.5 h. The amounts of carbon monoxide strongly adsorbed (v_{CO}) and those at the pressure of 20 kPa are also listed in Table 2.

4. Discussion

Although the XRD patterns show that the crystallites of nickel oxide are scarcely present in the catalysts except 50 wt.%Ni–S, the broad XPS peaks at ca. 856 eV for Ni $2p_{3/2}$ suggest the presence of considerable quantities of cationic nickel species on the surface of the catalysts [29,34]. The sharp peaks at ca. 853 eV are attributed to metallic nickel [29,34]. The binding energies for $NiSiO_3$ and NiO are reported as 856.9 and 854.0–854.9 eV, respectively [29,34]. The observation of the IR band at 960 cm^{-1} attributed to Ni–O–Si indicates the presence of interaction between nickel particles and the silica support. It is consistent with the presence of the broad XPS peak at ca. 856 eV because the electronic state of nickel in Ni–O–Si should be similar to that of $NiSiO_3$. The broad peak could be due to oxygen adsorbed in air or NiO on the surface; however, no significant change in the spectrum was observed even after deep sputtering, appearing that nickel oxide species on the surface is not responsible for the broad peak. Nickel oxide is apparently present in 50 wt.%Ni–S and it is consistent with the high ratio of broad and sharp peaks for Ni $2p_{3/2}$. The binding energy of the broad peak for 50 wt.%Ni–S is the closest to that for NiO [26,34], suggesting that the broad peak is due to both nickel oxide and nickel interacting with the support.

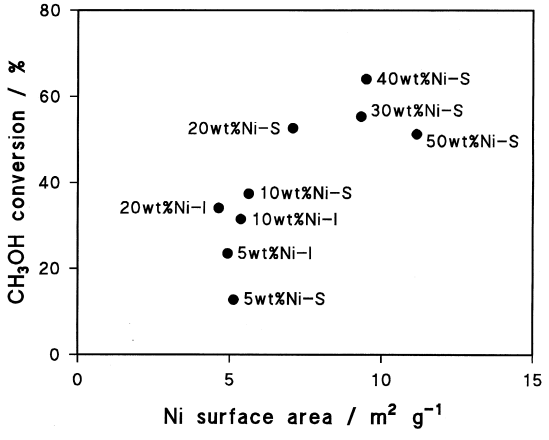

Fig. 9. Plot of nickel surface area vs. the methanol conversion.

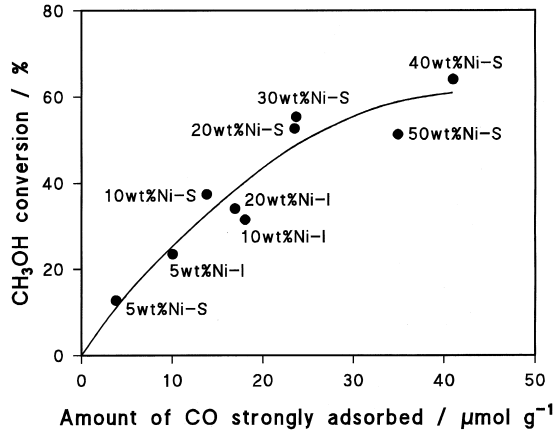

Fig. 10. Relationship between the amount of carbon monoxide strongly adsorbed and the methanol conversion.

The catalytic activity of metal particles on a support often relates to the surface area of the metal. However, the catalytic activity in the methanol decomposition does not always depend on the surface area of nickel (Fig. 9). Although the surface areas of nickel for 5 wt.%Ni–S, 10 wt.%Ni–S, 5 wt.%Ni–I, 10 wt.%Ni–I, and 20 wt.%Ni–I are close (4.9–5.6 $m^2\ g^{-1}$), the methanol conversions range from 12.8% to 37.4%, while no significant difference was observed in the XPS of these samples. It is noteworthy that the catalysts containing very small nickel particles with the size of 2–4 nm give low efficiency as seen in Fig. 9, especially in the case of 5 wt.%Ni–S of which nickel crystallite size is only 2.1 nm.

On the other hand, the activity relates well to the amount of carbon monoxide strongly adsorbed (Fig. 10). The catalytic activity also relates to the amount of hydrogen strongly adsorbed (Fig. 11). Although hydrogen is atomically adsorbed on a nickel atom, the quantity of

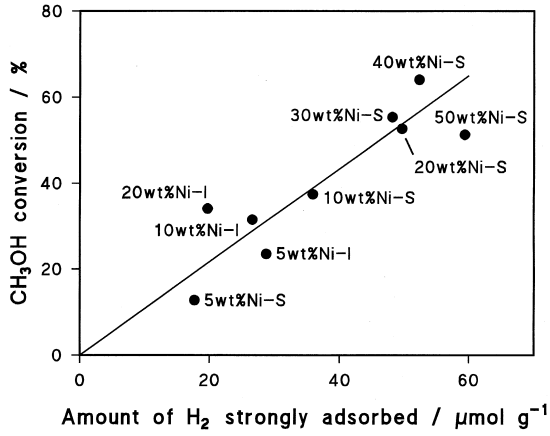

Fig. 11. Relationship between the amount of hydrogen strongly adsorbed and the methanol conversion.

hydrogen strongly adsorbed is larger than that of carbon monoxide strongly adsorbed (see Table 2). Two adsorption species, i.e., bridge (Ni_2CO) and linear (NiCO) are known as the species for carbon monoxide strongly adsorbed on nickel [35–37]. The stoichiometry in the quantities of adsorbed hydrogen and carbon monoxide suggests that the major species of carbon monoxide strongly adsorbed is the bridge type. Yasumori et al. [4] observed a promotional effect of hydrogen in the methanol decomposition over nickel and proposed that the rate determining step is the interaction between a surface methoxyl group and an adsorbed hydrogen atom. This implies that plural nickel atoms participate in the reaction step, and it can be supposed that the smooth surface of metallic nickel is rather advantageous for presence of such sites. Yates and Garland [35] showed that small nickel particles on silica cannot adsorb carbon monoxide strongly and that carbon monoxide is strongly adsorbed on nickel particles which are well crystallized. The characterization of the samples shows that nickel particles interact with the support via Ni–O–Si bonding. Thus, it is reasonable that crystallinity of very small nickel particles are poor, and they are less active than well-crystallized nickel particles on which both carbon monoxide and hydrogen are strongly adsorbed.

5. Conclusions

The catalytic activity of nickel supported on silica for the methanol decomposition to carbon monoxide and hydrogen at 250°C relates to the quantities of carbon monoxide and hydrogen strongly adsorbed on the catalyst, while the relationship between the activity and the surface area of nickel on the support is not evident. The catalysts containing very small nickel particles of which size is 2–4 nm is less active. This suggests that methanol decomposition is promoted on well-crystallized nickel particles of which surface strongly adsorb carbon monoxide and hydrogen. A significant part of nickel atoms on the surface are in contact with the silica support via bonding such as Ni–O–Si. Hence, the crystallinity of very small nickel particles is poor and their activity is low. The sol–gel technique is advantageous in the preparation of the catalysts with high metal loadings because it enables a good dispersion of a large number of nickel particles whose size is not very small.

References

[1] W. Keim (Ed.), Catalysis in C1 Chemistry, Reidel, Dordrecht, Holland, 1983.
[2] J.M. Fox III, Catal. Rev.-Sci. Eng. 35 (1993) 169.
[3] National Research Council, Catalysis Looks to the Future, National Academy Press, Washington, DC, 1992.
[4] I. Yasumori, T. Nakamura, E. Miyazaki, Bull. Chem. Soc. Jpn. 40 (1967) 1372.
[5] I. Yasumori, E. Miyazaki, Nippon Kagaku Kaishi 92 (1971) 659.
[6] S. Kasaoka, T. Shiraga, Nenryo Kyokaishi 59 (1980) 40.
[7] H. Niiyama, S. Tamai, J.-S. Kim, E. Echigoya, Sekiyu Gakkaishi 24 (1981) 322.
[8] A. Tada, T. Yoshino, H. Itoh, Chem. Lett. (1987) 419.
[9] M. Akiyoshi, H. Hattori, K. Tanabe, Sekiyu Gakkaishi 30 (1987) 156.
[10] M. Shimizu, K. Nobori, S. Takeoka, Kagaku Kogaku Ronbunshu 14 (1988) 114.
[11] M. Akiyoshi, H. Hattori, Sekiyu Gakkaishi 31 (1988) 239.
[12] Y. Nakazaki, T. Inui, Ind. Eng. Chem. Res. 28 (1989) 1285.
[13] M. Shimizu, S. Takeoka, Kagaku Kogaku Ronbunshu 15 (1989) 284.
[14] O. Tokunaga, Y. Satoh, T. Fukushima, S. Ogasawara, Sekiyu Gakkaishi 33 (1990) 173.
[15] H. Imai, T. Tagawa, K. Nakamura, Appl. Catal. 62 (1990) 348.

[16] H. Imamura, T. Takada, S. Kasahara, S. Tsuchiya, Appl. Catal. 58 (1990) 165.
[17] A. Tada, Y. Watarai, K. Takahashi, Y. Imizu, H. Itoh, Chem. Lett. (1990) 543.
[18] T. Okubo, M. Watanabe, K. Kusakabe, S. Morooka, Key Eng. Mater. 61/62 (1991) 71.
[19] M. Morita, K. Takeda, S. Tanabe, Y. Matsuda, Nippon Kagakukaishi (1991) 1238.
[20] M. Watanabe, T. Okubo, K. Kusakabe, S. Morooka, Ind. Eng. Chem. Res. 31 (1992) 2633.
[21] B. Chen, J.L. Falconer, J. Catal. 144 (1993) 214.
[22] K.J. Yoon, K.S. Jeong, J.E. Yie, Hwahak Konghak 31 (1993) 569.
[23] Y. Matsumura, K. Kagawa, Y. Usami, M. Kawazoe, H. Sakurai, M. Haruta, J. Chem. Soc., Chem. Commun. (1997) 657.
[24] J.-P. Jacobs, L.P. Lindfors, J.G.H. Reintjes, O. Jylha, H.H. Brongersma, Catal. Lett. 25 (1994) 315.
[25] H. Tamagawa, K. Oyama, T. Yamaguchi, H. Tanaka, H. Tsuiki, A. Ueno, J. Chem. Soc., Faraday Trans. 1 83 (1987) 3189.
[26] A. Ueno, H. Suzuki, Y. Kotera, J. Chem. Soc., Faraday Trans. 1 79 (1983) 127.
[27] J.L. Carter, J.A. Cusumano, J.H. Sinfelt, J. Phys. Chem. 70 (1966) 2257.
[28] H.P. Klug, L.E. Alexander, X-ray Diffraction Procedures, Wiley, New York, 1954.
[29] C.D. Wagner, W.M. Riggs, L.E. Davis, J.F. Moulder, G.E. Muilenberg (Eds.), Handbook of X-ray Photoelectron Spectroscopy, Perkin-Elmer, MN, 1978.
[30] JCPDS file, 4-0850 and 4-0835.
[31] H. Suzuki, S. Takasaki, F. Koga, A. Ueno, Y. Kotera, T. Sato, N. Todo, Chem. Lett. (1982) 127.
[32] J. Wong, C.A. Angell, Glass Structure by Spectroscopy, Marcel Dekker, New York, 1976.
[33] J.W.E. Coenen, Appl. Catal. 75 (1991) 193.
[34] D. Briggs, M.P. Seah (Eds.), Practical Surface Analysis, 2nd edn., Vol. 1, Auger and X-ray Photoelectron Spectroscopy, Wiley, New York, 1990.
[35] J.T. Yates, C.W. Garland, J. Phys. Chem. 65 (1961) 617.
[36] C.E. O'Neill, D.J.C. Yates, J. Phys. Chem. 65 (1961) 901.
[37] M. Primet, J.A. Dalmon, G.A. Martin, J. Catal. 46 (1977) 25.